A Photonic MEMS Accelerometer with a Low-Finesse Hemispherical Microcavity Readout

Yiliang Bao, Feng Zhou, Thomas W. LeBrun, and Jason J. Gorman
National Institute of Standards and Technology, Gaithersburg, MD USA
gorman@nist.gov

***Abstract*—This paper describes the design, fabrication, and testing of a photonic MEMS accelerometer that uses a hemispherical microcavity to transduce the motion of the proof mass. The cavity design provides stable operation that is relatively tolerant of misalignment errors. The prototype sensor is shown to have optical resonances that closely match the expected Airy function model.**

Keywords—Hemispherical microcavity; Fabry-Pérot; accelerometer; photonic MEMS.

I. Introduction

The design and testing of a new photonic MEMS accelerometer that uses Fabry-Pérot interferometry (FPI) to transduce acceleration will be described. FPI is a compelling candidate for transduction in accelerometers since it is highly accurate and sensitive and requires minimal surface area compared to capacitive, piezoresistive, and piezoelectric techniques. FPI has been studied for MEMS accelerometers by several groups [1-4]. However, these designs have focused on plane-parallel cavities, which suffer from poor optical coupling stability and lower effective finesse. The design presented in this paper uses a hemispherical cavity with high quality mirrors, resulting in significantly more stable sensing compared to the plane-parallel cavities found in previous work. The fabrication process for this design allows for the inclusion of high reflectivity coatings for optical cavities with high finesse but only uncoated low-finesse cavities will be discussed here.

II. Accelerometer Design

The basic accelerometer concept was previously described in [5] and is shown in Fig. 1. The accelerometer consists of two silicon chips that are fabricated separately and then bonded together to build the sensor. The chips are assembled on a standard fiber-optic mount to provide simple optical coupling into the cavity. The first chip contains a concave micromirror and the other chip contains a proof mass, which is suspended by silicon nitride beams along both the top and bottom edges. This structural design ensures that the higher order modes (rocking modes) are well separated from the fundamental mode (piston mode). Finite element analysis (FEA) shows that the resonance frequency of the first higher mode is at least 10 times higher than that of the fundamental mode, as shown in Fig. 2.

A variety of suspended proof masses have been fabricated with lengths ranging from 1 mm to 5 mm. To simplify the parameter variations, all designs use a 20 µm beam width, 1.5 µm beam thickness, and 500 µm proof mass thickness. The fundamental resonant frequency of the proof mass is set by varying the beam length from 40 µm to 110 µm and the proof mass width.

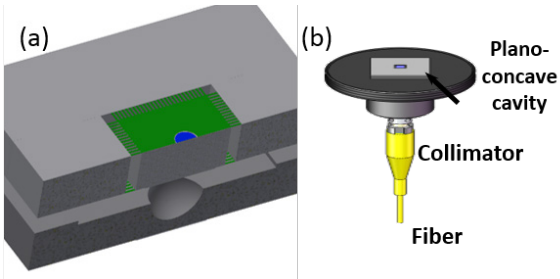

Fig. 1. Accelerometer design. (a) Exploded cross-sectional view showing the suspended proof mass and hemispherical microcavity, (b) fiber-optic sensor packaging.

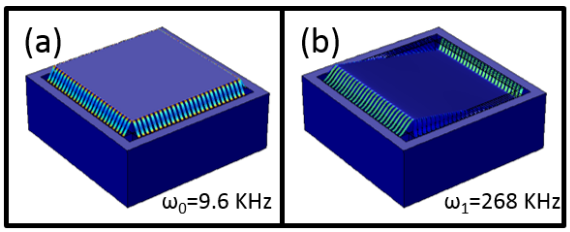

Fig. 2. Proof mass vibrational modes calculated using COMSOL Multiphysics. (a) Fundamental piston mode, (b) first rocking mode.

III. Fabrication

The hemispherical mirror is etched using HNA etching [5] and a silicon nitride hard mask with circular apertures. The radius of curvature and depth of the fabricated hemispherical mirrors are optimized to achieve the best mode matching insensitivity to fabrication variations while achieving a reasonable reduction in the power density on the mirrors, thereby mitigating stability issues related to laser heating. This is done by tuning the ratio of the depth to the radius of curvature to approximately 0.5. A typical mirror is shown in Fig. 3. The surface roughness is approximately 1 nm RMS, characterized using both an optical profilometer and AFM. The fabrication process for the suspended proof mass is shown in Fig. 4, which requires a complex etch that combines DRIE and KOH to release the proof mass and beams. A typical suspended proof mass is shown in Fig. 5.

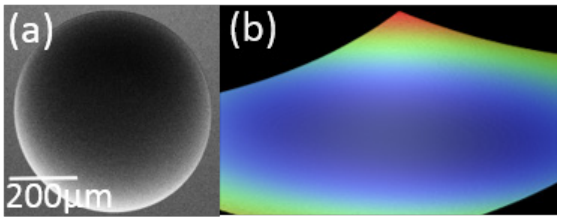

Fig. 3. Etched hemispherical mirror: (a) SEM top view, (b) 3D image from optical profilometer.

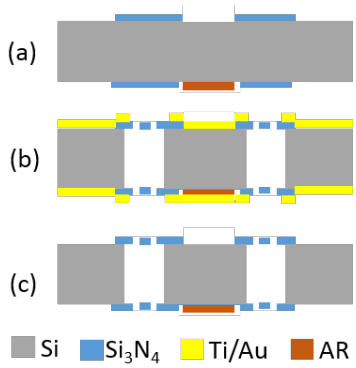

Fig. 4. Fabrication process for the suspended proof mass: (a) low-stress Si_3N_4 is patterned on silicon wafer and AR coating is deposited using a liftoff process, (b) Au mask is patterned using liftoff process for masking during KOH etch. The beams are patterned using RIE for Si_3N_4. DRIE is used to etch through the Si and KOH releases the beams. (c) Au mask is removed.

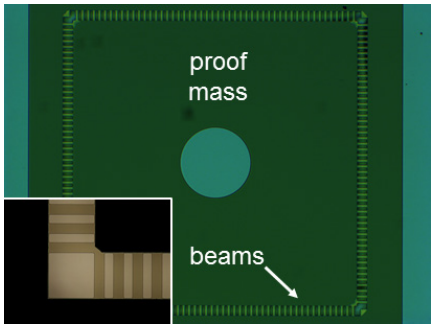

Fig. 5. Top view of a fabricated suspended proof mass where the inset shows a close-up of the beams.

IV. Results

The two chips have been bonded using an acrylic adhesive but future sensors will be assembled using fusion bonding, which will provide better thermal stability. The bonded chip is aligned on the fiber coupled package, as shown in Fig. 1(b), to form a portable accelerometer. The motion of the proof mass is measured by detecting shifts in the optical resonances of the cavity. A tunable laser is used to measure the transmission signal of the optical cavity as a function of the laser wavelength. Figure 6 shows the response of one optical cavity, where the transmitted and reflected signals are fit to an Airy function in order to extract the displacement information of the cavity length. On resonance, the cavity length change, dz_m, is translated into a wavelength change, $d\lambda$, as $dz_m/z_m = d\lambda/\lambda$. By evaluating the optical spectrum at the Airy function's point of maximum slope, we can determine the linearized transmission displacement sensitivity. Preliminary results for this cavity yield displacement and acceleration sensitivity of 1.8 mV/nm and 4.86 mV/g, respectively. Additional performance results for the accelerometer will be reported in the final presentation, including noise floor and shaker tests.

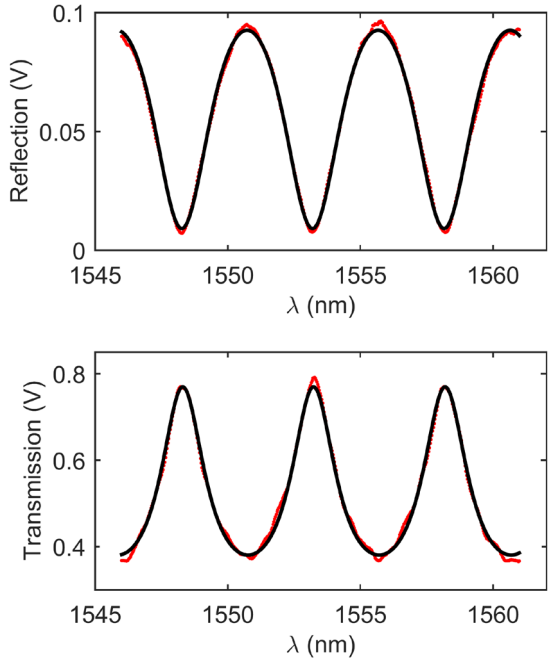

Fig. 6. Reflected and transmitted intensity of the hemispherical optical cavity as a function of laser wavelength. Red dots are the measured signal and the black lines are the fits to the standard Airy function model.

Acknowledgment

This research was performed in part in the NIST Center for Nanoscale Science and Technology Nanofab.

References

[1] R.L. Waters and M.E. Aklufi, "Micromachined Fabry–Perot interferometer for motion detection," Appl. Phys. Lett., vol. 81, pp. 3320-3322, 2002.

[2] M.A. Perez and A.M. Shkel, "Design and demonstration of a bulk micromachined fabry–pérot µg-resolution accelerometer," IEEE Sens. J, vol. 7, pp. 1653 – 1662, 2007.

[3] M.D. Pocha, G.A. Meyer, C.F. McConaghy, S.P. Swierkowski, J.D. Wolfe, "Miniature accelerometer and multichannel signal processor for fiberoptic Fabry–Pérot sensing," IEEE Sens. J., vol. 7, pp. 285-292, 2007.

[4] E. Davies, D.S. George, M.C. Gowera, and A.S. Holmes, "MEMS Fabry–Pérot optical accelerometer employing mechanical amplification via a V-beam structure," Sens. Actuators, A, vol. 215, pp. 22-29, 2014.

[5] Y. Bao, et al., "An optomechanical accelerometer with a high-finesse hemispherical optical cavity," *IEEE Int. Symp. Inertial Sensors and Systems*, Laguna Beach, CA, 2016, pp. 105-108.